Extreme Mechanics Letters 28 (2019) 22–30

Contents lists available at ScienceDirect

Extreme Mechanics Letters

journal homepage: www.elsevier.com/locate/eml

Extreme enhancement of interfacial adhesion by bulk patterning of sacrificial cuts

Ahmed Ghareeb, Ahmed Elbanna *

Department of Civil and Environmental Engineering, University of Illinois at Urbana–Champaign, Urbana, IL, 61801, USA

ARTICLE INFO

Article history:
Received 15 January 2019
Received in revised form 28 January 2019
Accepted 28 January 2019
Available online 10 February 2019

Keywords:
Sacrificial cuts
Interfacial adhesion
Bioinspired material

ABSTRACT

Many biological materials, such as bone and nacre, gain their strength and toughness through the formation of sacrificial bonds and hidden length structures. Here, inspired by these structural features, we propose a new mechanism for enhancing the interfacial adhesion toughness between an elastic body and a rigid substrate through patterning sacrificial secondary cuts in the bulk elastic material. The proposed sacrificial cuts are designed to break prior to detachment, altering the load path in the material and adding more compliance to the system, thus, increasing the total amount of work required before detachment while enabling independent control of the peak stress amplitude. Numerically, we use the finite element method to show that interfacial adhesion may be extremely enhanced by using multiple layers of sacrificial cuts and we provide a simple analytical framework to explain the underlying mechanism. Furthermore, we show that the overall behavior is tunable by changing the geometric and material parameters of the sacrificial cuts. In particular, the total work of adhesion may be made to increase linearly with the number of layers of the cuts. We discuss our findings in the context of enhancing interfacial adhesion by modulating the bulk geometric properties.

1. Introduction

Manipulating interfacial response for enhanced adhesion properties is a problem of great interest to scientists and engineers. Controlled and tunable interfacial adhesion is desirable in several applications, including adhesive bonds, composite materials, and biomedical systems. Enhancing interfacial toughness has been classically considered from physical chemistry point of view. Properties like wetting, contact angle, and adhesion energy may be controlled by properly functionalizing the interface [1,2].

Recently, it has been increasingly apparent that mechanics plays as much an important role in this problem as chemistry. There has been a surge of interest in patterning interfaces by introducing periodic [3–5] or functionally graded material properties [6] along the interfaces. The non-uniformity of the fracture energy along the interface may be utilized to enhance the interfacial resistance to separation and delamination by increasing the effective toughness [7]. However, most studies regarding this approach requires special surface treatment to achieve the targeted interfacial properties.

Alternatively, some recent studies suggested enhancing interfacial adhesion properties by optimizing the distribution of interfacial stresses inspired by the biological example of fibrils with mushroom-shaped tips [8,9]. The results of these studies suggest that reducing the stress concentrations, which initiates the crack propagation, significantly improves the interfacial adhesion [10,11]. This idea was applied through using a composite fibril composed of a stiff stalk and a soft tip rounded layer to decrease the corner stress [12]. The interfacial stress may also be controlled by adding bulk voids near the interface [13]. Voids alter the stress field leading to non-uniform interfacial stress, which may lead to slowing down the crack and increasing the fracture toughness.

There has been an interest in Kirigami inspired tunable metamaterials. The material stretchability may be extremely enhanced by adding patterned cuts [14,15]. Patterned cuts change the load transfer mechanism from stretching of the material strip to bending of beams defined by horizontal cuts. The stretchability may be further increased by adding major and minor cuts to alter the boundary conditions of the beams and allow further rotation at the joints [16]. However, introducing cuts leads to significant reduction in the material strength and the stiffness [14]. Here, we propose the idea of sacrificial cuts to enhance the interfacial adhesion. Sacrificial cuts will enable having a two-phase material; a phase with high stiffness and strength, followed by a phase of high stretchability and thus energy dissipation prior to total detachment from the substrate.

We draw our inspiration from the concept of sacrificial bonds and hidden length existing in nature. Many biological and polymeric materials, such as bone and abalone shells, gain strength and fracture toughness through the formation of these dynamic structural features [17–22]. Sacrificial bonds often connect two

* Corresponding author.
E-mail address: elbanna2@illinois.edu (A. Elbanna).

https://doi.org/10.1016/j.eml.2019.01.011
2352-4316/

different sites within the material bulk constraining them from stretching. These bonds have weak strength relative to the strength of the material, hence they break before the material rupture adding more ductility to the material system and increasing the total amount of work required to break the material. In this paper, we propose to enhance the interfacial adhesion toughness through patterning sacrificial cuts in the bulk material. Similar to sacrificial bonds and hidden lengths mechanism, these sacrificial cuts are to break prior to failure altering the load path in the material and adding more compliance to the system, thus, increasing the total work required before detachment.

The remainder of the paper is organized as follows. In Section 2, we introduce the model setup and the finite element procedure. In Section 3, we summarize our results for the effect of single as well as multiple layers of bulk patterned sacrificial cuts. We also present a simple analytical model that explains the adhesion enhancement mechanism. Finally, we discuss the implications of our model and results in Section 4.

2. Model setup

We start by investigating the effect of a single layer of near-interface sacrificial cuts on the detachment behavior of a plate from a rigid substrate. Fig. 1(a) shows the setup of our model. It is composed of three parts: (i) a rigid base plate that represents the substrate, (ii) a plate with a row of sacrificial cuts near the interface where the faces of the sacrificial cuts are initially bonded using a zero-thickness cohesive layer and (iii) a zero-thickness cohesive layer joining the two components to represent the adhesion between the plate and the substrate. The dimensions of the base plate are chosen in a way that the boundaries have no effect on the results. The lower edge of the base plate is restrained from movement in both directions. A uniform upward displacement is applied at the top edge of the plate. The plate material is assumed to be linear elastic, isotropic, and homogeneous.

Finite element simulations:

To model the cohesive interface, we use a zero-thickness cohesive element. We adopt a simple intrinsic triangular cohesive law for mode I fracture composed of a linear elastic part up to the critical cohesive stress σ_{cr}, followed by linear degradation that evolves from crack initiation to complete failure. The analytical expression for the cohesive law is given by [23]:

$$\sigma(\Delta) = \begin{cases} K_o \Delta, & \Delta \leq \gamma \Delta_f \\ \sigma_{cr}(\Delta_f - \Delta)/(\Delta_f - \gamma \Delta_f), & \gamma \Delta_f \leq \Delta \leq \Delta_f \\ 0, & \Delta \geq \Delta_f \end{cases} \quad (1)$$

where K_o is penalty stiffness of the cohesive law, Δ_f is the normal displacement corresponding to total separation, and γ is the ratio between the critical and the failure normal displacements, the details of the traction separation relation are shown in Fig. 1(c). K_o value is determined by selecting proper values of σ_{cr} and γ. The total area under the curve is the cohesive fracture energy G_c, and the length on which stress changes from σ_{cr} (crack initiation) to 0 (total separation) defines the process zone length l which is related to the characteristic length L_{ch} of the cohesive zone law given by [24]:

$$L_{ch} = \frac{E G_c}{{\sigma_{cr}}^2} \quad (2)$$

where E is young's modulus of the bulk material, G_c is the cohesive model energy release rate, and σ_{cr} is the maximum allowed stress. This is a fundamental length scale in our problem that controls the solution dependence on the material properties. In this study, we consider sacrificial cuts that are many times longer than the cohesive zone length l.

We use the finite element software package ABAQUS [25]. We conduct Implicit dynamic analysis with slow loading rate to represent a quasi-static pulling test under displacement-controlled boundary conditions. The plate is meshed using 2D plane strain quadrilateral elements whereas the cohesive interface is meshed using zero thickness cohesive elements. The size of the cohesive elements is chosen to be $L_{pz}/50$ at most to avoid solution jump that may result in divergence or global oscillations [26]. We have conducted a mesh sensitivity analysis to ensure adequate accuracy.

All simulations presented in the results section were run using the following set of parameters: For the bulk material, the Young's modulus = 500 MPa, and Poisson's ratio = 0.45. For the cohesive law representing the adhesion between the bulk material and the substrate, the critical cohesive stress (S_{int}) = 10 MPa, cohesive fracture energy = 500 J/m^2, and γ = 0.5. For the cohesive law representing the cohesion between the sacrificial cut faces, the critical cohesive stress (S_c) = αS_{int} where α ranges between 0 and 1. All other cohesive law parameters are kept the same as the interfacial adhesion properties. The nominal stress σ_n is calculated as the total plate force divided by the interfacial contact area, and the nominal strain ε_n is calculated as the top vertical displacement divided by the total plate height in the undeformed configuration (L_p).

3. Results

3.1. Effect of a single layer of sacrificial cuts

Fig. 2(a) shows the effect of adding a single layer of sacrificial secondary cuts on the overall nominal stress vs. nominal strain response of the plate. For small nominal strains, the cuts remain intact and fully transfer the load to the primary interface leading to a response indistinguishable from the solid plate. However, once the nominal stress reaches the value of the critical cohesive stress of the sacrificial cut (S_c), which is lower than the critical cohesive stress of the main interface (S_{int}), the sacrificial cuts start debonding. This corresponds to the first peak and the subsequent drop in the nominal stress curve. The sacrificial cuts then open up leading to a response similar to the case of cohesive-less cuts (S_c = 0). The nominal stress increases till the initiation of interfacial debonding, which corresponds to the second peak in the nominal stress curve. Following that, the nominal stress decreases gradually with the propagation of the interfacial crack till full detachment. The breakage of the sacrificial cuts increases the system compliance and increases the total energy dissipated before the failure.

Fig. 2(b) shows the stress distribution along the interface at different nominal strain values and a schematic of the deformed shape at a representative time in the post-peak loading phase. Initially, when the cuts are closed, the stress is uniform. As the plate is loaded, the stress keeps increasing till it reaches the critical stress of the sacrificial cut, then the sacrificial cuts open and the stress along the interface becomes non-uniform. When the stress reaches the cohesive strength of the main interface, local interfacial cracks start propagating under the vertical strips, where the stress is highest, into regions of lower stress. This crack trapping mechanism reduces the crack growth speed and enables further stretching of the plate and enhanced ductility. Eventually, the cracks coalesce leading to complete separation of the interface. We note that the peak nominal stress in the plates with cuts is tunable by the critical cohesive stress of the sacrificial cuts. Thus, the proposed design enables higher stretchability, similar to kirigami plates, but without significantly reducing the overall strength.

In Appendix A, we present a theoretical analysis for the response of systems with single layer of cohesive-less cuts. We use a model based on extensible Euler–Bernoulli beam theory to confirm that adding horizontal cohesive-less cuts near the interface enhances the stretchability prior to failure but reduces the

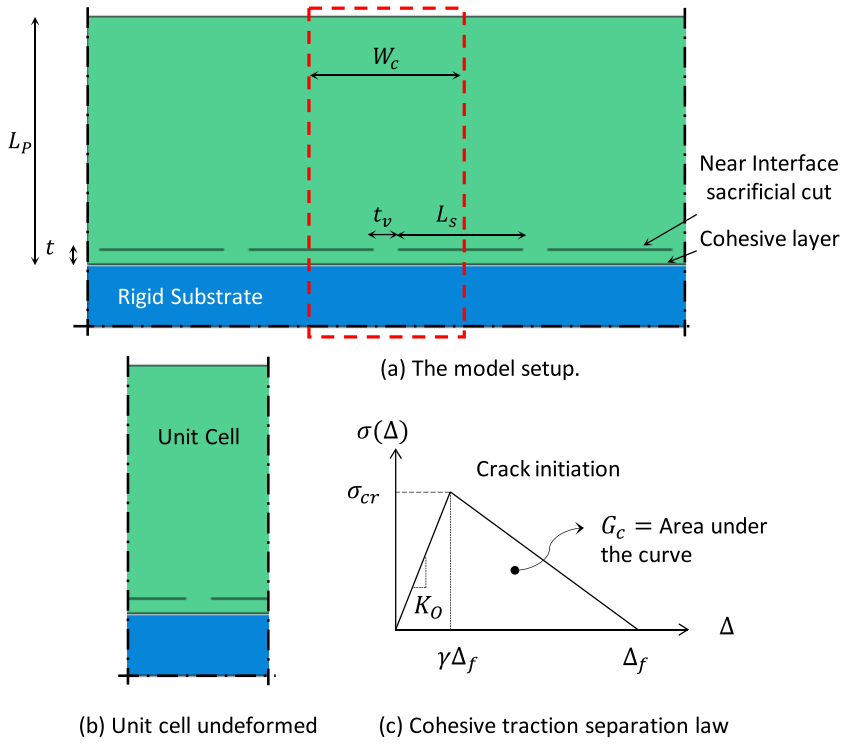

Fig. 1. The model setup: (a) The geometry of the model: a plate with a row of near interface sacrificial cuts adhered to a rigid substrate through a zero-thickness layer of cohesive material, (b) unit cell of the plate at the undeformed configuration, and (c) The traction separation curve for the cohesive law used in the finite element simulations.

nominal stress. The effect of bulk cuts, in the single layer layout, is significant only if the distance between the interface and the cut t is small compared to the cut length L_s. Furthermore, we show that for large t/L_S ratios, snap instabilities may occur leading to sudden failure that releases kinetic energy providing another pathway for energy dissipation.

The separation pattern and stress–strain relation is qualitatively similar to the case of cavitation in the adhesive layer and formation of fibrils [27,28]. The cavitation/fibril formation processes help dissipate energy and thus increases toughness. However, the void formation and growth in these cases remain largely stochastic and susceptible to internal defect distributions. A systematic design from the beginning, as proposed here, may achieve better toughening results with a higher level of control. This may be particularly relevant for improving adhesion in soft polymeric materials including emerging ones such as hydrogels.

3.2. Effect of multiple layers of patterned cuts

The results in the previous section show that adding a single layer of sacrificial cuts near the interface leads to enhancing the maximum stretch before failure without significant reduction of the peak strength. The same idea may be extended for multiple layers of cuts to further increase the stretchability and fracture toughness.

Fig. 3(a) shows the effect of using multiple layers of sacrificial cuts, the nominal stress vs. nominal strain curves for both solid plate and plate with cohesive-less cuts having the same outer dimensions, and number of cut layers are added for reference. The figure shows that adding sacrificial cuts led to having a saw tooth behavior, the first peak nominal stress depends on S_c/S_{int} ratio, whereas the following behavior depends on both S_c/S_{int} and the beam thickness to length ratio t/L_s. The plate stiffness reduces after each peak due to the formation of a new beam which adds more compliance to the system. Furthermore, for this case, the stress drops abruptly once the interfacial crack initiates (Point 8 in Fig. 3(a)), and does not exhibit a tail similar to the case of a single layer of sacrificial cuts (Fig. 2(a)). This may be explained as follows, due to the existence of multiple layers, the plate is highly stretched prior to interfacial debonding, and once interfacial crack initiates, the plate fully detaches with a snap as the top part of the plate unloads and pulls the interfacial strip up. This snapping behavior is discussed thoroughly in Appendix A and suggests that part of the energy will be dissipated as kinetic energy. Fig. 3(b) shows the deformed shape of the unit cell at different loading stages. The unit cell is fully attached at the beginning and acts as a solid plate, however, after the first peak nominal stress, sacrificial cuts start to open in sequence with each new formed crack corresponding to a peak in the stress–strain curve till full detachment.

The evolution of the interfacial stress distribution for the case of multiple layers of sacrificial cuts is shown in Supplementary Material. The stress is uniform at the beginning, and as the sacrificial cuts open, the stress becomes non-uniform. The stress then keeps fluctuating following the saw tooth behavior shown in Fig. 3(a) till the interfacial separation initiates. After that sudden detachment occurs. This behavior is qualitatively similar to the case of a single layer of sacrificial cuts shown in Fig. 2(b).

Fig. 4 shows the effect of changing the layer spacing in the vertical direction. The figure shows the nominal stress vs. nominal strain relation for 3 cases, a solid plate, a plate with 7 layers of sacrificial cuts with $t/L_s = 0.125$, and plate with 7 layers of sacrificial cuts with $t/L_s = 0.25$. The figure shows that layers with larger thickness require higher peak nominal stress to form a new sacrificial layer. However, the overall stretchability and hence the fracture toughness in this case is lower than the plate with smaller layers thickness to cut length ratio ($t/L_s = 0.125$). Contours of the bulk von-Mises stress distribution in both cases are shown in the same plot. For thin layers, the stress distribution shows that force is mainly transferred by bending. However, for the thick layers, the force is transferred by stretching of X-shaped formed struts.

The results presented in Fig. 4 show the principle conclusion of this paper: patterning the sacrificial cuts and controlling their dimensions and critical cohesion stress lead to material systems with

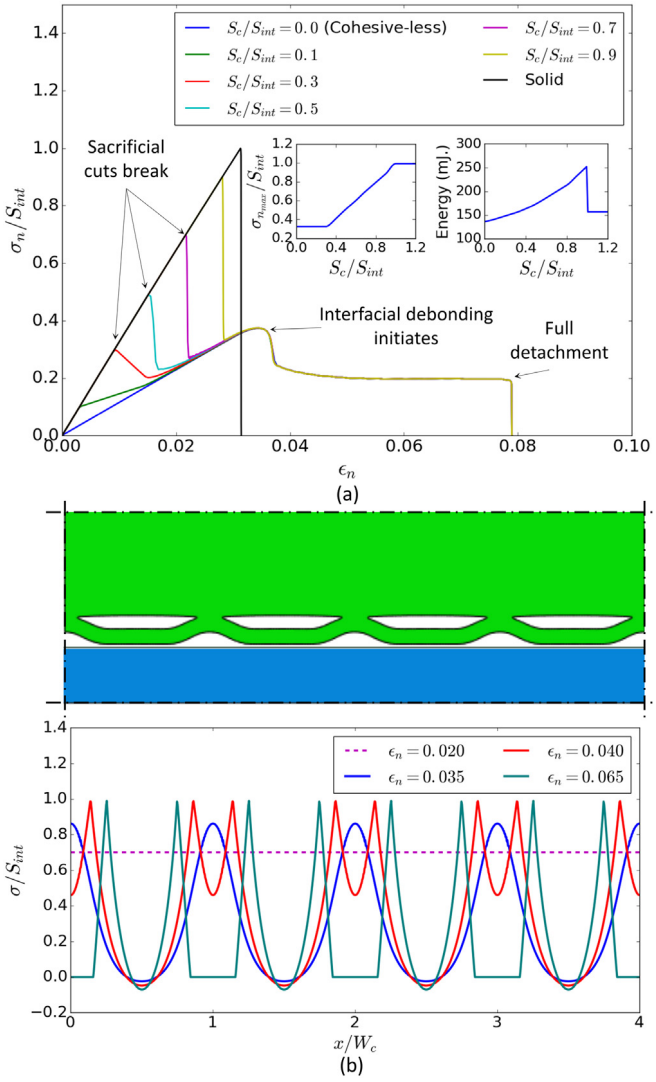

Fig. 2. The effect of adding a single layer of sacrificial cuts on the macroscopic stress–strain curve and the interfacial debonding: (a) The nominal stress to interface critical stress ratio vs. nominal strain for different sacrificial cut critical stress to interface critical stress ratios for $t/L_s = 0.20$. The two inserts show the enhancement in the peak nominal stress and the area under the curve, and (b) the separation pattern at the interface, and the normalized stress distribution along the interface at different values of nominal strains for $S_c/S_{int} = 0.7$ and $t/L_s = 0.20$. (For interpretation of the references to color in this figure legend, the reader is referred to the web version of this article.)

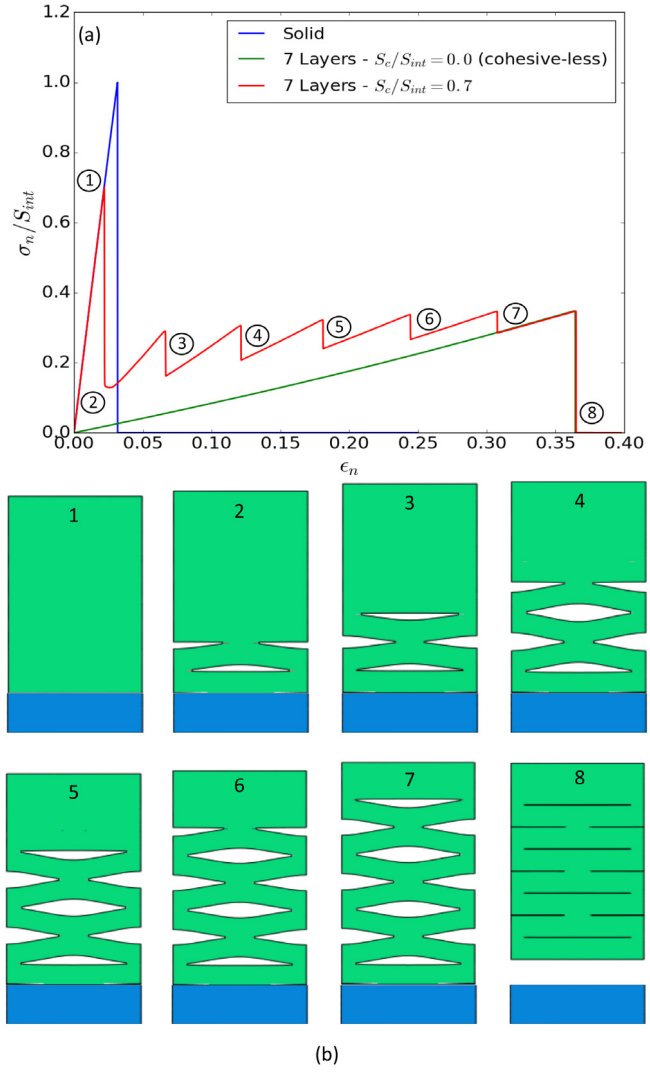

Fig. 3. Using multiple layers of staggered sacrificial cuts: (a) The nominal stress to interface critical stress ratio vs. nominal strain for a solid plate, plate with cohesive-less cuts with $t/L_s = 0.125$, and a plate with sacrificial cuts with $S_c/S_{int} = 0.7$, and $t/L_s = 0.125$, and (b) the deformed shape of the unit cell showing the progression of layers detachment. (For interpretation of the references to color in this figure legend, the reader is referred to the web version of this article.)

enhanced interfacial fracture toughness, where the peak strength, the average stress of the tail, the maximum stretch and the total area under the curve may be tuned and maximized. The curves show that the height of the tail (average stress of the tail) is controlled by the layer thickness. However, both the maximum stretchability and energy dissipated, i.e. the total area under the curve, are mostly controlled by t/L_s ratio and both scale nearly linearly with the number of layers as shown in the insert.

A simple analytical model:

To analyze the response of the plate with multiple layers of sacrificial cuts, we consider the following two phases for the system:

Phase 1: Fully attached layers: The unit cell, shown in Fig. 5(b), is idealized as a set of springs in series, each spring represent a fully attached layer. Since all layers are fully attached, the load is transferred directly through stretching where the unit cell acts like an axial member. The stiffness for each attached layer is $K_i = EA/t_i$, and the stiffness of the unit cell is the equivalent stiffness of all layers in series. This is equal to $K = EA/L_p$.

Phase II: Initiation of sacrificial cuts: After the uniform stress in the unit cell exceeds the critical stress of the sacrificial cuts, a sacrificial cut detaches changing the load transfer mechanism. The load is transferred through bending in the newly formed beam instead of stretching. This adds more compliance to the system which leads to sudden drop in the nominal stress. In this limit, the system is idealized as a set of blue springs (which represent fully attached layer), and red springs (which represent detached layers) connected in series. When a sacrificial cut detaches after reaching the critical load, the equivalent spring changes from blue to red till all sacrificial cuts are detached. The sequence is shown in Fig. 3(b).

For the idealized spring representing the beam that formed due to the opening of a secondary cut (red spring), the same theoretical procedure discussed in Appendix A for the Euler–Bernoulli beam may be used to predict an approximation for the force required to detach the sacrificial cut. At the failure initiation, the normal

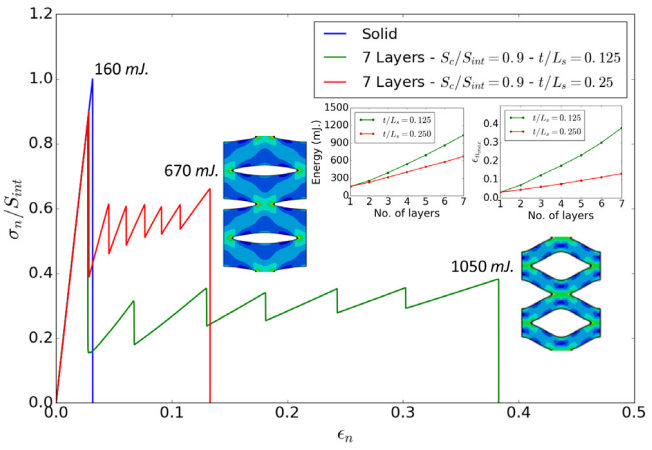

Fig. 4. The effect of the layer thickness on the normalized nominal stress vs. nominal strain behavior. The von-Mises stress distribution and the total area under the curve are shown in the figure. The inserts show the scaling of the maximum nominal strain and the total area under the curve with the number of sacrificial cuts (layers). (For interpretation of the references to color in this figure legend, the reader is referred to the web version of this article.)

force in the beam may be neglected as the beam is still under small deformation assumption. Solving Eq. (A.1) with $N = 0$ and the boundary conditions at crack initiation, the force required to open up a sacrificial cut is approximated by:

$$P = \sqrt[4]{\frac{2048}{9} EIb^3\sigma_{cr}^3 v_o} \tag{3}$$

where b is the plate thickness out of plane, I is the moment of inertia of the layer, and σ_{cr}, v_o are the parameters for Dugdale's traction separation law for the sacrificial cut. This approximate relation shows that increasing the layer thickness leads to increasing the force required to open a sacrificial cut (i.e. the peak nominal stress of the sawtooth behavior shown in Fig. 3(a)). Under the same assumption, the initial slope of the force displacement curve of the beam when it starts loading is:

$$K_{in.} = \frac{192EI}{L_s^3} = 16bE\left(\frac{t}{L_s}\right)^3 \tag{4}$$

However, this value of $K_{in.}$ for each single idealized beam (red spring) is not constant and increases with increasing the beam's vertical deflection, as shown in Fig. 5(c), due to the stiffening effect of the normal force in the beam. This approximate relation shows that increasing the layer thickness to the cut length ratio significantly increases the stiffness. Although Eqs. (3), (4) are approximate, they qualitatively agree with the numerical results shown in Fig. 4. Furthermore, using these approximate relations for the two idealized springs (red and blue), the simple spring-in-series model may also be used to approximately predict the reduction of the macroscopic stiffness associated with the successive detachment of the sacrificial interfaces as observed in Figs. 3(a) and 4.

4. Discussion

In this paper we introduce the idea of nature-inspired sacrificial cuts to enhance the adhesion properties of architected materials. Similar to the concept of sacrificial bonds and hidden lengths in many nature and polymeric materials, the sacrificial cuts fail prior to the global failure of the system adding more compliance and allowing more energy dissipation before the failure.

The idea of shielding or toughening using microcracks in the crack tip near field has been investigated for different materials where the existence of microcracks was found to enhance the fracture toughness of brittle materials. [29–31]. In addition,

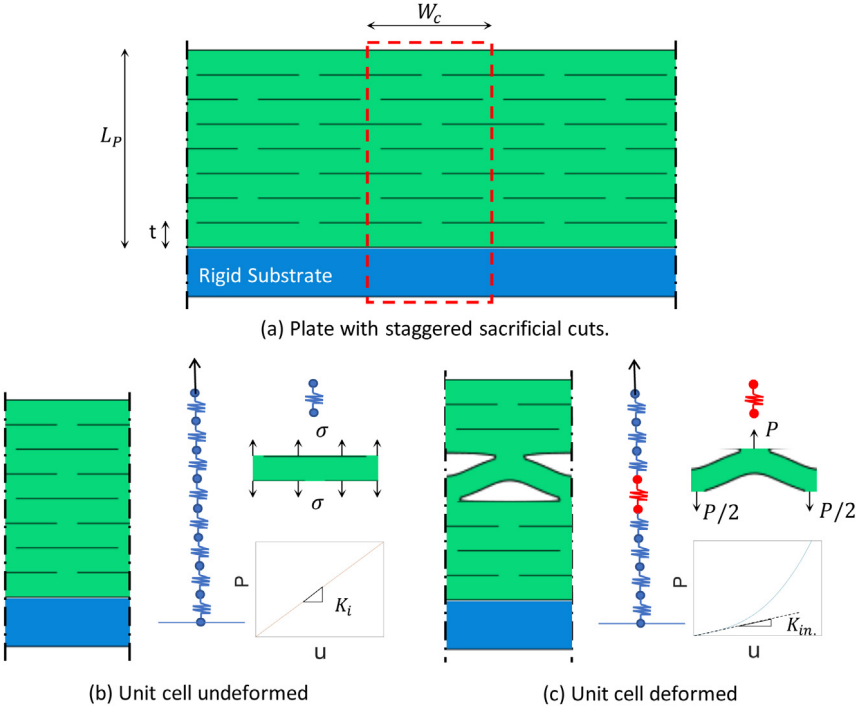

Fig. 5. The geometry and idealization of the plate with staggered sacrificial cuts: (a) The geometry of the plate, (b) The unit cell in the undeformed configuration where all layers are attached, each layer is loaded axially thus it may be idealized as a spring with a linear stiffness of nearly EA/L, and (c) The unit cell in the deformed configuration after reaching the stress that opens a sacrificial cut, the layer is loaded through bending and may be idealized as extensible Euler–Bernoulli beam. The force displacement relation for both idealized springs are shown in the figure. (For interpretation of the references to color in this figure legend, the reader is referred to the web version of this article.)

the fracture toughness and subcritical crack growth resistance of material interfaces were found to be enhanced by introducing controlled arrays of microcrack-voids out-of-plane to the main interfacial crack [32]. Furthermore, Kirigami inspired materials with patterned cuts were found to have enhanced deformability that can be tuned by changing the cut parameters [14–16]. In adhesion problem, introducing cuts in the bulk material near the interface leads to non-uniform stress along the interface, leading to changing the detachment mechanism from stretching to peeling of thin material strips. Thus, changing the failure pattern and increasing the peak stretch values before the failure. However, the enhancement of the stretchability is accompanied with significant reduction in the peak strength compared to solid plate.

The sacrificial cuts solve this problem by allowing the material to have two phases. The first phase is before the failure of the sacrificial cuts in which the material behavior is similar to that of a solid plate and the peak strength is relatively high (may be made arbitrary close to the strength of a solid plate). The second phase begins when the bulk stress reaches that of the sacrificial cut. At that point, the sacrificial cut debonds, adding more compliance to the material and changing its behavior to a plate with open cuts (Kirigami-like), leading to higher stretchability before failure. Thus, introducing sacrificial cuts leads to adhesion response with high ductility and toughness with controllability on the detachment force compared to a solid plate.

By adding multiple layers of sacrificial cuts, the adhesion energy may be further increased. The successive opening of the sacrificial cuts leads to a stress–strain curve with a saw tooth like character with each failing layer adding more compliance to the system and increasing the overall stretchability and energy dissipation, which may be useful for some important applications in soft materials such as wet adhesives [33] and stretchable electronics [34,35]. The behavior may be tuned by changing the material parameters, such as the ratio between the critical stress of the sacrificial cut and the interface with the substrate, or geometric parameters such as the cut length and spacing in both directions. The ratio between the strength of the sacrificial cut and the interface with the substrate controls the peak strength of the plate which corresponds to first peak in the saw tooth behavior. By approaching a ratio of 1, the peak strength of the plate with sacrificial cuts approaches that of a solid plate. However, if the ratio becomes 1 or greater, the material detaches from the substrate prior to any sacrificial cut breakage, thus the sacrificial cuts have no effect on the behavior.

Furthermore, the geometric parameters of the sacrificial cuts have significant effect on the behavior. When the spacing between the cuts in the direction perpendicular to the interface increases compared to the cut length (i.e. t/L_s increases), the saw tooth behavior tends to have higher stress peaks in the tail and less ductility, i.e. shorter tails. For lower values of t/L_s, the tail becomes longer but with smaller stress peaks. This is because of a transition from a stretch dominated (for high t/L_s) to bending dominated (for low t/L_s) response. For high t/L_s, sacrificial cuts require higher force to break. After breakage, the force is transferred by stretching of X-shaped formed struts, thus the plate is stiffer. For low t/L_s, sacrificial cuts require lower force to break and the force is transferred, after breakage, as bending, leading to a more compliant response. Most notably, the adhesion energy, for a wide range of parameters, increases almost linearly with the number of layers opening new pathways for extreme enhancement of interfacial adhesion.

In our work, we have assumed that the bulk material does not undergo any damage or plasticity. This assumption holds for the cases where the critical cohesive stress and the fracture toughness of both the sacrificial cuts and the interface with the substrate are low compared to the material strength and fracture toughness. We have chosen cohesive fracture energy and critical cohesive stress to be lower than the mean of the corresponding values of rubber-like materials [36]. As part of the future work, we plan to investigate failure in the bulk as a possible competing mechanism.

The concept of sacrificial cuts may be applied to enhance the adhesion properties of soft materials, specially for systems subjected to dynamic loadings, or in applications where extreme stretchability is desired. Our results suggest a rich behavior that is tunable by careful design of the geometric and material parameters of the sacrificial cuts. While the current work is largely theoretical, the system of sacrificial cuts may be realized experimentally using different techniques including multi-material additive manufacturing [37] to fabricate a layered material with patterned weakened zones or by varying the degree of curing of the polymeric material using temperature or light [38,39] which leads to spatially varying material properties.

Future extensions of this work may include studying other patterns of sacrificial cut distribution, exploring the effect of materials nonlinearity, large deformation, plasticity, and damage, as well as studying the loading rate effect. Other extensions of this work may include studying the effect of uncertainty in material properties and studying the effect of sacrificial cuts mechanism in 3D where the sacrificial cuts may be distributed in the two dimensions differently providing additional control on the adhesion directional dependence.

Acknowledgments

This research has been supported by funds from Campus Research Board of University of Illinois Urbana–Champaign, United States (RB17043), and the National Science Foundation, United States grant (CAREER Award Number 1753249).

Appendix A. Semi-analytical modeling of systems with a single layer of cohesive-less cuts and validation using FEM

As a starting point for our analysis, we compare the pulling behavior of a unit cell of an elastic plate, with and without a cohesive-less cut ($S_c = 0$), adhered to a rigid substrate. The plate material is assumed to be linear elastic, isotropic, and homogeneous. Cohesive zone model (CZM) is used to model the adhesion between the plate and the substrate. The cohesive layer is assumed to follow Dugdale's traction separation relation with a constant critical stress σ_{cr}, and max displacement v_o. Furthermore, we consider cuts that are many times longer than the cohesive zone length l. The model does not allow damage in the plate material and failure occurs only due to detachment via adhesive failure at the interface. The details of the model setup are shown in Fig. A.1(a)

For the case of solid plate, the force is transferred vertically through stretching the unit cell till the applied stress reaches the critical stress $\sigma = \sigma_{cr}$, the nominal strain at the peak stress is given by $\varepsilon = E\sigma_{cr}$. After reaching the critical stress, the plate will completely detach from the substrate. For the case of a plate with cuts, the model can be discretized to two parts as shown in Fig. A.1(b), the top part of the plate and the interfacial strip. The top part may be idealized as a spring with stiffness K_v that is calculated from the material properties and unit cell dimensions using finite element method, whereas the interfacial strip may be idealized as an extensible Euler–Bernoulli beam on elastic foundations. This assumption holds when the interfacial strip thickness is small compared to its length.

Due to symmetry, we analyze only half of the interfacial beam, the model is shown in Fig. A.1(c). The vertical displacement is governed by the equation [40]:

$$-EI\frac{d^4w}{dx^4} + N\frac{d^2w}{dx^2} + q = 0 \tag{A.1}$$

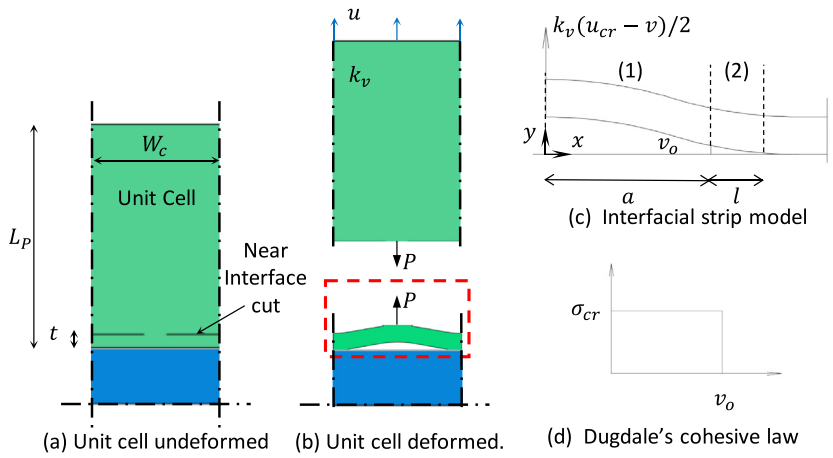

Fig. A.1. Setup of the theoretical model: (a) a unit cell of a plate with a single row of near interface cuts adhered to a rigid substrate through a zero-thickness layer of cohesive material, (b) discretization of the unit cell as top part and interfacial strip, (d) the model of the interfacial beam on elastic foundation, and (e) Dugdale's cohesive traction separation law.

where w is the vertical displacement, N is the normal force in the beam and q is the distributed force per unit length of the beam. The normal force is given by:

$$N = EA\left[\frac{du}{dx} + \frac{1}{2}\left(\frac{dw}{dx}\right)^2\right] \tag{A.2}$$

where u is the horizontal displacement of the beam. Integrating both sides and applying the symmetry boundary conditions around the vertical axis.

$$N = \frac{EA}{2L}\int_0^L \left(\frac{dw}{dx}\right)^2 dx \tag{A.3}$$

where L is the beam length. It is worth noting that for moderately large rotations, the equation of equilibrium in the horizontal direction is not affected hence, N is constant. We rewrite Eq. (A.1) as:

$$\frac{d^4w}{dx^4} - \lambda^2\frac{d^2w}{dx^2} = \frac{q}{EI} \tag{A.4}$$

With

$$\lambda^2 = \frac{N}{EI} \tag{A.5}$$

The solution to this equation is given by

$$w = C_1 + C_2x + C_3e^{\lambda x} + C_4e^{-\lambda x} - \frac{1}{\lambda^2}\frac{q}{2EI}x^2 \tag{A.6}$$

We have two zones, the debonded zone (zone (1) in Fig. A.1(c)) for which $q = 0$. And the process zone (zone (2) in Fig. A.1(c)) with length l and downward distributed force of $b\overline{\sigma}$. Since we are using Dugdale's traction separation relation, the beam is fully attached behind the process zone. The two zones give two equations with 8 unknowns, in addition to the vertical upward displacement u_{cr}, the normal force N and the process zone length l, a total of 11 unknowns. The boundary conditions used to solve the problem are:

$$\begin{aligned} &\text{At } x = 0,\ v' = 0,\ \text{and } v''' = K_v(u_{cr} - v)/2EI \\ &\text{At } x = a,\ v = v_o \\ &\text{At } x = a + l,\ v = v' = v'' = 0 \end{aligned} \tag{A.7}$$

In addition to the four continuity conditions at the interface between zones 1, and 2. When the crack front approaches the symmetry boundary conditions, the value of l becomes determined as $l = W_c/2 - a$, and the boundary conditions at $x = a + l$ change to $v' = v''' = 0$. These equations are solved numerically to get the relation between the nominal stress and the nominal strain. The results of the theoretical model are compared to the finite element results in Fig. A.2(a).

Fig. A.2(a) shows the normalized nominal stress vs. nominal strain from both the finite element and the extensible Euler Bernoulli beam models for a solid plate, a plate with a cut with $t/L_s = 0.225$, and a plate with a cut with $t/L_s = 0.425$ where t is the thickness of the interfacial strip, L_s is the length of the cut. The theoretical model predicts slightly higher peak nominal stresses due to the assumption that the force is concentrated at one point. The finite element models also did not capture the unloading part of the curve due to the displacement-controlled nature of loading in the FEM where the boundary displacement increases monotonically and is not allowed to decrease. Thus, FEM models fail upon reaching the peak displacement. Otherwise, the results show good agreement.

When the interfacial debonding initiates, the elastic top part of the plate (above the cut) is unloaded, thus it starts to pull the interfacial strip, even if the top displacement is still constant. For the cases when t/L_s is small, or when the stiffness of the top part of the plate K_v is high compared to the stiffness of the interfacial strip, the peak nominal strain is controlled by the vertical displacement of the interfacial beam, as shown in the case when $t/L_s = 0.225$. However, when t/L_s becomes large, or K_v is small (very long plate for example). The peak displacement is controlled by the deflection of the plate at detachment initiation as shown in the case when $t/L_s = 0.425$. The plate is fully detached as soon as it reaches the peak nominal stress with a snap, releasing kinetic energy.

Fig. A.2(b) shows the effect of the interfacial strip thickness to the cut length ratio t/L_s on the normalized nominal stress vs. nominal strain relation of the plate. For small ratios, the interfacial crack initiates under the edge vertical strips at low nominal stress value, however, the peak displacement at failure is increased due to the small rigidity of the interfacial strip. With increasing the thickness ratio, the nominal stress value at crack initiation increases.

Fig. A.2(c) shows that the normalized nominal stress increases asymptotically with increasing the interfacial strip thickness approaching the value of 1. This suggests that the influence of the cut on the peak nominal stress decreases with increasing t/L_sratio. Fig. A.2(d) shows a non-monotonic trend as the peak nominal strain reduces with increasing t/L_s, but when the value of t/L_s is 0.4, the peak nominal strain value starts to slightly increase approaching an asymptotic value. The same trend is observed for the energy dissipation (i.e. Total area under the curve) as shown in Fig. A.2(e) where the inflection point is at t/L_s around 0.35.

The non-monotonic response in Fig. A.2(d) and (e) reflects a transition between two regimes: (i) a regime in which the peak

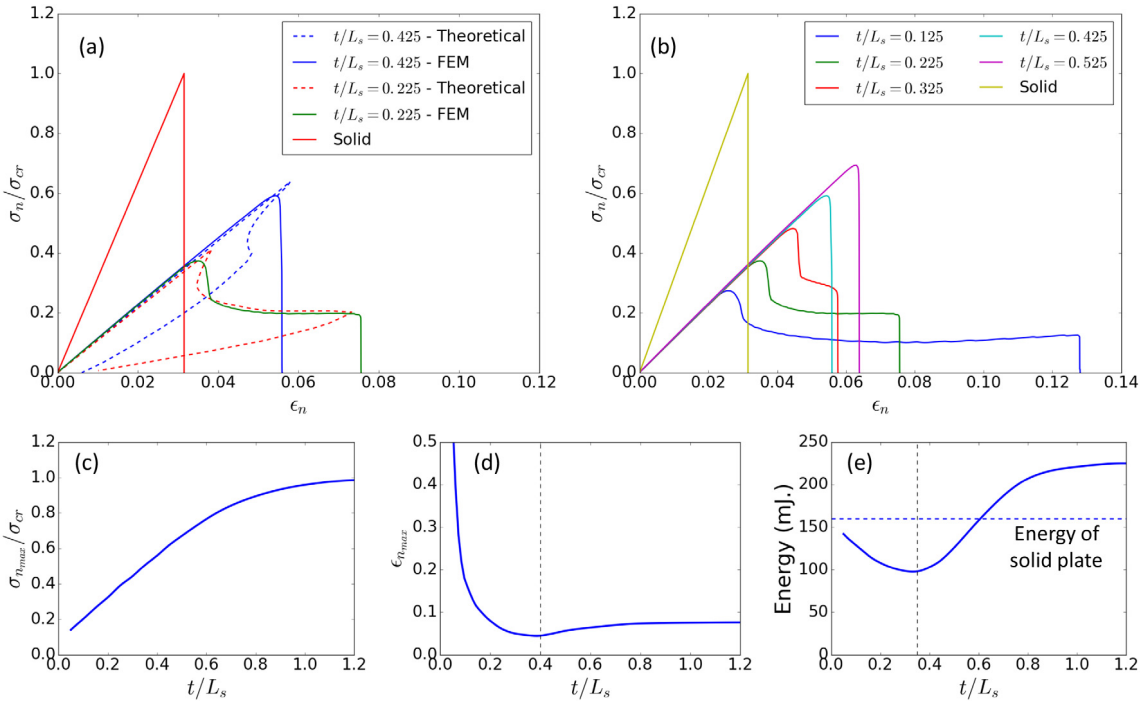

Fig. A.2. The effect of adding near interface cut: (a) The nominal stress to interface critical stress ratio vs. nominal strain for the case of solid plate, and two plates with a layer of near interface cuts with different interfacial strip thickness to cut length ratio (t/L_s) using the theoretical model and finite element simulations, and (b) the effect of the interfacial strip thickness to length ratio on the nominal stress vs. nominal strain relations, (c) The effect of the interfacial strip thickness to cut length ratio on the peak nominal stress, (d) The effect of the interfacial strip thickness to length ratio on the peak nominal strain, and (d) The effect of the interfacial strip thickness to length ratio on the total area under the curve. (For interpretation of the references to color in this figure legend, the reader is referred to the web version of this article.)

nominal strain is controlled by the interfacial beam deflection, and (ii) another regime in which the peak nominal strain is controlled by the plate deformation. When the response is controlled by the interfacial beam deflection, the peak nominal strain significantly increases with decreasing t/L_s. The dissipated energy value also increases with decreasing t/L_s but at a lower rate since the peak nominal stress decreases with decreasing t/L_s. In addition, when t/L_s value increases approaching 1, the peak nominal stress and strain tend to approach a constant value, and the behavior becomes independent on the value of t/L_s. This suggests that introducing cuts in the bulk material, even if the cuts are cohesive-less, may lead to a very rich behavior that may be further leveraged in tuning interfacial adhesion.

This appendix shows that introducing cohesive-less cuts in the bulk material close to the interface may lead to enhanced stretchability prior to failure, however, the peak nominal stress is significantly decreased compared to a solid plate. As discussed in Section 3.1, the idea of sacrificial cuts may solve this problem by combining high peak nominal stress and high peak nominal strain, leading to an overall increase in interfacial toughness.

Appendix B. Supplementary data

Supplementary material related to this article can be found online at https://doi.org/10.1016/j.eml.2019.01.011.

References

[1] B.P. Lee, P.B. Messersmith, J.N. Israelachvili, J.H. Waite, Mussel-inspired adhesives and coatings, Annu. Rev. Mater. Res. 41 (1) (2011) 99–132.
[2] H. Lee, B.P. Lee, P.B. Messersmith, A reversible wet/dry adhesive inspired by mussels and geckos, Nature 448 (7151) (2007) 338–341.
[3] T. Suzuki, R. Matsuzaki, A. Todoroki, Y. Mizutani, Prediction of the macroscopic fracture toughness of a composite/adhesive interface with periodic surface microstructures, Int. J. Adhes. Adhes. 60 (2015) 16–22.
[4] W.S. Kim, I.H. Yun, J.J. Lee, H.T. Jung, Evaluation of mechanical interlock effect on adhesion strength of polymermetal interfaces using micro-patterned surface topography, Int. J. Adhes. Adhes. 30 (6) (2010) 408–417.
[5] N.J. Glassmaker, A. Jagota, C.-Y. Hui, W.L. Noderer, M.K. Chaudhury, Biologically inspired crack trapping for enhanced adhesion, Proc. Natl. Acad. Sci. 104 (26) (2007) 10786–10791.
[6] M. Heß, A simple method for solving adhesive and non-adhesive axisymmetric contact problems of elastically graded materials, Internat. J. Engrg. Sci. 104 (2016) 20–33.
[7] A.S. Childers, N.R. Brodnik, K.T. Faber, Interfacial frictional stresses and fracture toughness of biomorphic graphite/copper interfaces, Mater. Lett. 174 (2016) 106–109.
[8] A. Del Campo, C. Greiner, E. Arzt, Contact shape controls adhesion of bioinspired fibrillar surfaces, Langmuir 23 (20) (2007) 10235–10243.
[9] C. Greiner, A. Del Campo, E. Arzt, Adhesion of bioinspired micropatterned surfaces: Effects of pillar radius, aspect ratio, and preload, Langmuir 23 (7) (2007) 3495–3502.
[10] S.N. Khaderi, N.A. Fleck, E. Arzt, R.M. McMeeking, Detachment of an adhered micropillar from a dissimilar substrate, J. Mech. Phys. Solids 75 (2015) 159–183.
[11] N.A. Fleck, S.N. Khaderi, R.M. McMeeking, E. Arzt, Cohesive detachment of an elastic pillar from a dissimilar substrate, J. Mech. Phys. Solids 101 (2017) 30–43.
[12] R.G. Balijepalli, S.C.L. Fischer, R. Hensel, R.M. McMeeking, E. Arzt, Numerical study of adhesion enhancement by composite fibrils with soft tip layers, J. Mech. Phys. Solids 99 (2016) (2017) 357–378.
[13] A. Ghareeb, A. Elbanna, On the role of the plaque porous structure in mussel adhesion: Implications for adhesion control using bulk patterning, J. Appl. Mech. 85 (12) (2018) 121003.
[14] T.C. Shyu, P.F. Damasceno, P.M. Dodd, A. Lamoureux, L. Xu, M. Shlian, M. Shtein, S.C. Glotzer, N.A. Kotov, A kirigami approach to engineering elasticity in nanocomposites through patterned defects, Nature Mater. 14 (8) (2015) 785–789.
[15] M. Isobe, K. Okumura, Initial rigid response and softening transition of highly stretchable kirigami sheet materials, Sci. Rep. 6 (April) (2016) 1–6.
[16] D.G. Hwang, M.D. Bartlett, Tunable mechanical metamaterials through hybrid kirigami structures, Sci. Rep. 8 (1) (2018) 1–8.
[17] G.E. Fantner, T. Hassenkam, J.H. Kindt, J.C. Weaver, H. Birkedal, L. Pechenik, J.A. Cutroni, G.A.G. Cidade, G.D. Stucky, D.E. Morse, P.K. Hansma, Sacrificial bonds and hidden length dissipate energy as mineralized fibrils separate during bone fracture, Nature Mater. 4 (8) (2005) 612–616.

[18] P.K. Hansma, G.E. Fantner, J.H. Kindt, P.J. Thurner, G. Schitter, P.J. Turner, S.F. Udwin, M.M. Finch, Sacrificial bonds in the interfibrillar matrix of bone, J. Musculoskelet. Neuronal Interact. 5 (4) (2005) 313–315.
[19] G.E. Fantner, E. Oroudjev, G. Schitter, L.S. Golde, P. Thurner, M.M. Finch, P. Turner, T. Gutsmann, D.E. Morse, H. Hansma, P.K. Hansma, Sacrificial bonds and hidden length: Unraveling molecular mesostructures in tough materials, Biophys. J. 90 (4) (2006) 1411–1418.
[20] C.K.C. Lieou, A.E. Elbanna, J.M. Carlson, Sacrificial bonds and hidden length in biomaterials: A kinetic constitutive description of strength and toughness in bone, Phys. Rev. E (3) 88 (1) (2013) 12703.
[21] A.E. Elbanna, J.M. Carlson, Dynamics of polymer molecules with sacrificial bond and hidden length systems: Towards a physically-based mesoscopic constitutive law, PLoS One 8 (4) (2013) 1–10.
[22] W. Wang, A. Elbanna, Crack propagation in bone on the scale of mineralized collagen fibrils: Role of polymers with sacrificial bonds and hidden length, Bone 68 (2014) 20–31.
[23] F. Furgiuele, A. Leonardi, C. Maletta, G.H. Paulino, Fracture analysis of adhesive joints using intrinsic cohesive zone models, Congr. IGF19 (2007) 77–84.
[24] K. Ha, H. Baek, K. Park, Convergence of fracture process zone size in cohesive zone modeling, Appl. Math. Model. 39 (19) (2015) 5828–5836.
[25] Abaqus Analysis User's Manual, 6.13th ed. Dassault Systemes Simulia Corp. Providence, RI, USA, 2013.
[26] A. Turon, C.G. Dávila, P.P. Camanho, J. Costa, An engineering solution for mesh size effects in the simulation of delamination using cohesive zone models, Eng. Fract. Mech. 74 (10) (2007) 1665–1682.
[27] A.J. Crosby, K.R. Shull, H. Lakrout, C. Creton, Deformation and failure modes of adhesively bonded elastic layers, J. Appl. Phys. 88 (5) (2000) 2956–2966.
[28] C. Creton, H. Lakrout, Micromechanics of flat-probe adhesion tests of soft viscoelastic polymer films, J. Polym. Sci. B 38 (7) (2000) 965–979.
[29] J.W. Hutchinson, Crack tip shielding by micro-cracking in brittle solids, Acta Metall. 35 (7) (1987) 1605–1619.
[30] M. Rühle, A.G. Evans, R.M. McMeeking, P.G. Charalambides, J.W. Hutchinson, Microcrack toughening in alumina/zirconia, Acta Metall. 35 (11) (1987) 2701–2710.
[31] D.K.M. Shum, J.W. Hutchinson, On toughening by microcracks, Mech. Mater. 9 (2) (1990) 83–91.
[32] T.S. Oh, J. Rödel, R.M. Cannon, R.O. Ritchie, Ceramic/metal interfacial crack growth: Toughening by controlled microcracks and interfacial geometries, Acta Metall. 36 (8) (1988) 2083–2093.
[33] J. Li, A.D. Celiz, J. Yang, Q. Yang, I. Wamala, W. Whyte, B.R. Seo, N.V. Vasilyev, J.J. Vlassak, Z. Suo, D.J. Mooney, Tough adhesives for diverse wet surfaces, Science (80-) 357 (6349) (2017) 378–381.
[34] J.A. Rogers, T. Someya, Y. Huang, Materials and mechanics for stretchable electronics, Science (80-.) 327 (5973) (2010) 1603 LP–1607.
[35] J.A. Fan, W.H. Yeo, Y. Su, Y. Hattori, W. Lee, S.Y. Jung, Y. Zhang, Z. Liu, H. Cheng, L. Falgout, M. Bajema, T. Coleman, D. Gregoire, R.J. Larsen, Y. Huang, J.A. Rogers, Fractal design concepts for stretchable electronics, Nature Commun. 5 (2014) 1–8.
[36] E. Dragoni, G. Medri, Fracture toughness evaluation of natural rubber, Theor. Appl. Fract. Mech. 10 (1) (1988) 79–83.
[37] R.L. Truby, J.A. Lewis, Printing soft matter in three dimensions, Nature 540 (7633) (2016) 371–378.
[38] M. Miyazaki, Y. Oshida, B. Keith Moore, H. Onose, Effect of light exposure on fracture toughness and flexural strength of light-cured composites, Dent. Mater. 12 (5–6) (1996) 328–332.
[39] D. Incerti, T. Wang, D. Carolan, A. Fergusson, Curing rate effects on the toughness of epoxy polymers, Polymer (Guildf). 159 (October) (2018) 116–123.
[40] J.N. Reddy, An Introduction to Nonlinear Finite Element Analysis, 91, 2004.